

1 **Long-term variability of the South China Sea mixed layer**
2 **salinity over the past six decades**

3
4
5
6 **Lili Zeng^{1*}, Eric P. Chassignet² and Xiaobiao Xu²**

7
8
9 *1. State Key Laboratory of Tropical Oceanography (LTO), South China Sea Institute*
10 *of Oceanology, Chinese Academy of Sciences, Guangzhou, China*

11 *2. Center for Ocean-Atmospheric Prediction Studies, Florida State University,*
12 *Tallahassee, Florida*

13
14
15 Manuscript for the Journal of Geophysical Research (Oceans)

16
17
18
19
20
21
22 Corresponding Author:

23 Dr. Lili Zeng

24 State Key Laboratory of Tropical Oceanography, South China Sea Institute of
25 Oceanology, Chinese Academic of Sciences, Guangzhou, China

26
27 Tel: (86) 20- 8902-4304; Fax: (86)20-8902-4304

28 Email: zenglili@scsio.ac.cn

29 **Abstract**

30 A recently assembled South China Sea Physical Oceanographic Dataset (SCSPOD)
31 provides the first observational evidence for mixed layer salinity changes in the South
32 China Sea (SCS) from 1960 to 2015. During this period, the mixed layer waters
33 freshened by 0.22 psu. The mixed layer salinity variability is found to be in sync with
34 the Pacific Decadal Oscillation (PDO); it freshened in the 1960s, started to salinify in
35 1974, freshened again from 1993, and then salinified once again from 2012, with
36 linear trends of -0.019 , 0.020 , and -0.024 psu/yr, respectively. A box-average salinity
37 budget analysis shows that the surface forcing, horizontal advection, and vertical
38 entrainment terms together can, to a large degree, explain the observed trend in mixed
39 layer salinity. The mixed layer freshening is driven by weakened surface fresh water
40 loss and saline water transport, while salinification is associated with enhanced
41 surface freshwater loss and salt transport through the Luzon Strait. The long-term
42 mixed layer salinity changes affect the stratification, inducing a thinner mixed layer
43 and stronger barrier layer during freshening periods that favor stronger regional
44 ocean–atmosphere interaction.

45 **Key words:** South China Sea; mixed layer salinity; long-term variability

46

47

48

49

50

51

52 **1. Introduction**

53 The global water cycle is a key element of the climate system, yet it is poorly
54 understood primarily because most of it occurs over the vast and under-sampled
55 oceans (Schmitt, 1995; 2008). There is, however, ample evidence from salinity
56 observations and numerical results from climate models indicating that the water
57 cycle has changed over the past six decades (Wong et al., 1999; Munk, 2003) and that
58 it has intensified (Durack et al., 2012).

59 Ocean salinity is globally conserved and quantification of its variability is
60 essential to understanding the linkages between the water cycle and climate change
61 (Curry et al., 2003; Boyer et al., 2005; Schmitt and Blair, 2015). Salinity
62 measurements are used to diagnose changes in important components of the earth
63 climate dynamics, such as surface freshwater flux, freshwater transport, and ocean
64 mixing (Lukas and Lindstrom, 1991; Wijffels et al., 1992; Dickson et al 2002; Li et al,
65 2016ab). Robust and spatially coherent trends in salinity are found in the global ocean,
66 where surface salinity increases are observed in evaporation-dominated regions and
67 decreases are observed in precipitation-dominated regions (Durack et al., 2010; Skliris
68 et al., 2014).

69 An abundance of historical records combined with recent observations from
70 various programs have been used to document salinity changes throughout the globe.
71 Long hydrographic records show that the salinity changes in the North Atlantic can be

72 associated with significant changes in the North Atlantic Oscillation index (Dickson et
73 al., 2002; Häkkinen, 2002; Curry et al., 2003; Holliday et al., 2008; Sarafanov et al.,
74 2008). Combined surface measurements document Pacific Decadal Oscillation
75 (PDO)-like signals in sea surface salinity in the tropical Pacific (Delcroix et al., 2007;
76 Du et al., 2015; Nan et al., 2015). Recent observations in the Southern Indian Ocean
77 show a fast freshening since 1995 with a particularly striking acceleration since 2006
78 (Anilkumar et al., 2015; Menezes et al., 2017; Du et al., 2015).

79 The South China Sea (SCS) is the largest tropical marginal sea and has one of the
80 lowest average surface salinity levels (~33 psu) (Zeng et al., 2014). It is located in the
81 Indo-Pacific Ocean, identified by Durack et al. (2012) as one of the areas that
82 experienced the most significant freshening during the 1950-2000 period. The
83 temperature and salinity variations and controlling factors in the SCS are remarkably
84 different from those in the open ocean. The South China Sea Throughflow (SCSTF)
85 connects the Pacific and Indian Oceans, acts as an oceanic bridge, and strongly affects
86 the heat and freshwater budgets in the SCS (Qu et al., 2006; Wang et al., 2006; Liu et
87 al., 2012; Gordon et al., 2012). The SCSTF consists of inflow through the Luzon
88 Strait and outflows through the Karimata, Mindoro, and Taiwan Straits, respectively
89 (Figure 1). The large quantity of saline water brought through the Luzon Strait by the
90 SCSTF can contribute as much salinity variations in the SCS as the local freshwater
91 flux.

92 Due to the limited amount of observations, only a few studies have focused on

93 salinity changes in the SCS and most of the attention has been on the northern SCS
94 (Liu et al., 2012; Nan et al., 2013, 2016; Zhao et al., 2014; Zeng et al., 2014, 2016).
95 Nan et al. (2013, 2016) showed that the freshening in the northeastern SCS in the
96 1990s and 2000s was associated with a weakening trend of the Kuroshio intrusion.
97 Zeng et al. (2014) also found that the extreme freshening event in the northern SCS
98 during 2012 was caused by a weak Kuroshio intrusion. Year 2012 is also when a
99 20-year freshening trend was reversed (Zeng et al., 2018). Decadal variability has
100 been documented for subsurface salinity in the northern SCS during 1960 and 2012
101 (Zeng et al., 2016a). Finally, Liu et al. (2012) and Zhao et al. (2014) showed decadal
102 changes in intermediate waters along 18°N in the northern basin (Liu et al., 2012;
103 Zhao et al., 2014). However, very little is actually known about the decadal and
104 long-term variability for the SCS as a whole.

105 In this paper, we analyze a recent observational dataset with the aim of 1)
106 understanding the decadal and longer-term upper salinity changes in the SCS over the
107 past six decades and 2) assessing the factors that contribute to these changes using a
108 box-average mixed layer salinity budget analysis. The paper is organized as follows.
109 The data and variables used to compute the budget are presented in section 2. The
110 observed changes in salinity over the period 1960–2015 and the possible influence of
111 the PDO are presented in section 3. In section 4, the box-average mixed layer salinity
112 budget and the possible factors controlling variations in the mixed layer salinity are
113 documented. Finally, conclusion and discussions are given in section 5.

114 **2. Data and variables**

115 **2.1 In situ observational dataset**

116 The South China Sea Physical Oceanographic Dataset (SCSPOD14) consists of
117 validated in situ observations collected from the World Ocean Database 2009
118 (WOD09), Argo floats, and the South China Sea Institute of Oceanology (SCSIO)
119 measurements for the period 1919–2014 (Zeng et al., 2016b). This dataset has been
120 updated by adding quality-controlled Argo float and SCSIO cruise measurements
121 from 2015 (hereafter, SCSPOD15). Details of the data sampling characteristics,
122 processing method, and quality control of this dataset can be found in Zeng et al.
123 (2016b). We focus on the 1960–2015 period because the spatial and temporal coverage
124 of the observations is dense enough to document variability. Overall, 34,485 records
125 located deeper than 50 m within the well-sampled region (107–121°E, 3–23°N) are
126 used for the analysis (Figure 2a). The spatial distribution of the observations as a
127 function of longitude is shown in Figure 2b, as well as their sources: WOD09, Argo,
128 and SCSIO. There are no salinity observations in SCSPOD15 for the year 2003, and
129 several years in the mid-1960s have few observations. The interior basin (110–120°E)
130 is sampled quite well with only a few years of poor data coverage. However, in the
131 region west of 110°E, the sampling is quite sparse after the mid-1990s. The mixed
132 layer depth, mixed layer salinity, and barrier layer thickness are calculated for each
133 profile as described in detail by Zeng et al. (2016b).

134 **2.3 Variables**

135 To assess the impact of the air-sea freshwater flux ($E-P -R$, positive freshwater
136 flux indicates loss of freshwater from the ocean), we use the evaporation data from
137 the Objectively Analyzed air-sea Fluxes (OAFlux; Yu and Weller, 2007) together with
138 four precipitation products: the Precipitation Reconstruction (PREC; Chen et al.,
139 2002), the National Centers for Environmental Prediction's Climate Prediction Center
140 (CPC; Chen et al., 2002), the Global Precipitation Climatology Project (GPCP; Adler
141 et al., 2003), and the Tropical Rainfall Measuring Mission (TRMM; Huffman et al.,
142 2007). The four net freshwater $E-P$ flux datasets are hereafter referred to as PRECflux,
143 CPCflux, GPCPflux, and TRMMflux, respectively. The Mekong and Pearl river
144 runoffs are estimated from the river-basin-integrated precipitation as in Zeng et al.
145 (2014).

146 To assess the impact of the horizontal salt transport, ocean currents from several
147 products are used. They include the Simple Ocean Data Assimilation (SODA)
148 reanalysis data from 1960 to 2012 (Carton et al., 2008), the National Centers for
149 Environmental Prediction (NCEP) Global Ocean Data Assimilation System (GODAS)
150 reanalysis data from 1980 to 2012 (Huang et al., 2010), reanalysis data from 1993 to
151 2015 from the Hybrid Coordinate Ocean Model (HYCOM) data assimilative system
152 GOFS 3.1 (Chassignet et al., 2009; Metzger et al., 2014), quasi global OGCM for the
153 Earth Simulator (OFES) hindcast data from 1960 to 2010 (Sasaki et al., 2008), and
154 West Pacific (including the SCS) hindcast data from 1992 to 2015 using the Regional
155 Ocean Modeling Systems (ROMS; Xiu et al., 2010).

156 Finally, to assess the vertical entrainment, we use NCEP wind stress, OFES
157 vertical velocity outputs, and mixed layer depth calculated from SCSP0D15 profiles.

158 **3. Observed features**

159 **3.1 Salinity change between 1960 and 2015 (56 years)**

160 We start by first looking at the long-term salinity change in the upper 250 m from
161 1960 to 2015 (56 years). The longitudinally averaged salinity change in the SCS for
162 the upper 250 m was obtained using SCSP0D15 and its variability is displayed in
163 Figure 3a. Between 1960 and 2015, the salinity in the upper 50 m is marked by a
164 significant long-term decrease in salinity (0.22 psu), with an averaged trend of -0.20
165 psu/50yr (or -0.004 psu/yr). This freshening trend can extend as far down as 100 m in
166 the western SCS. In the east, the freshening near the Luzon Strait is even deeper
167 extending as far down as 250 m. Below the mixed layer (~50 m), there is an apparent
168 subsurface salinification beneath 100 m in the central basin between 110°E and 118°E.
169 Overall, the basin-wide averaged salinity shows that the SCS experienced a
170 significant freshening in the top 100 m and weak salinification in the subsurface
171 layers (Figure 3b). Regions where the freshening magnitude exceeds 0.004 psu/yr are
172 limited to the mixed layer waters.

173 The linear trends in mixed layer salinity are calculated on 2°×2° bins and are
174 displayed in Figure 4. The crosses indicate the bins in which the computations of
175 trends are not reliable using a Mann-Kendall test. Overall, the mixed layer salinity in
176 the SCS has been decreasing over the past 56 years, with an averaged trend of -0.15

177 psu/50yr (or -0.003 psu/yr). The freshening trend is stronger in the northern part of the
178 basin than in the southern basin. In the northeastern region, the long-term freshening
179 trend is about -0.175psu/50yr. This trend is comparable to the value east of the Luzon
180 Strait reported by Durack et al. (2012), i.e., -0.15 to -0.20 psu over a 50-year period
181 (1950–2000).

182 **3.2 Decadal variability**

183 The decrease in mixed layer salinity between 1960 and 2015 is not necessarily
184 linear; freshening during one time period could alternate with salinification during
185 another. To explore the decadal variability, we first show in Figure 5 the
186 temperature-salinity (T–S) diagram averaged basin-wide for each of the six decades.
187 These T – S curves are an effective way to distinguish freshening or salinification
188 periods (decades) from the climatological mean conditions. They show that the SCS
189 has experienced significant decadal variability over the past six decades. The upper
190 ocean salinity is highest in the 1990s and lowest in the 2010s. The great salinification
191 of the 1990s also occurred in the Atlantic, tropical Pacific, and Indian Ocean (Curry et
192 al., 2003; Delcroix et al., 2007; Skliris et al., 2014). These decadal differences can be
193 seen in all of the datasets (WOD09, SCSIO, and Argo) that comprise SCSP0D15.
194 Different datasets show important similarities in the decadal changes over the past
195 sixty years.

196 To further illustrate the variability of the salinity in the SCS, in Figure 6a we plot
197 yearly variations of basin-wide averaged salinity for the upper 250 m from 1960 to

198 2015. The upper ocean started to freshen in the 1960s and continued through the
199 mid-1970s. This was followed by a short salinification period in the late 1970s, then
200 freshening again until the mid-1990s. Significant freshening occurred yet again in the
201 2010s. This variability, which can be as high as 0.4 psu, is clearly visible in the
202 salinity anomaly plot (Figure 6b), with phases of high salinity in the 1960s and
203 mid-1990s and low salinity in the mid-1970s and the 2010s. The salinity anomalies
204 can extend down from the surface to about 200 m, but the highest anomalies with
205 amplitude of up to 0.4 psu are mostly confined to the mixed layer. We therefore now
206 focus on the mixed layer salinity variability.

207 **3.3 Mixed layer salinity variability**

208 Figure 7 shows longitude–time sections of mixed layer salinity from 1960 to
209 2015 averaged between 3°N and 23°N. There is a striking difference between the SCS
210 and Pacific waters east of 121°E. The mixed layer salinity in the SCS is significantly
211 lower than that of Pacific waters. As discussed in the previous section, the mixed
212 layer salinity underwent freshening in the 1970s, salinification during the 1980s and
213 1990s (~0.4 psu), and then freshening again. The lowest salinity was recorded in 2012
214 (Zeng et al., 2014). This is summarized by Figure 8, which shows the time evolution
215 of the basin-wide mixed layer salinity, including the one standard errors. The error bar
216 is estimated as the standard error of all mixed layer salinity values for a given
217 calendar year. The seven-year band pass time series (in blue) can be divided into four
218 periods separated by three mixed layer salinity minima and maxima: 1974 (the

219 secondary minimum mixed layer salinity), 1993 (the maximum mixed layer salinity),
220 and 2012 (the minimum mixed layer salinity). The observed change in mixed layer
221 salinity is first a decrease of about -0.4 psu during 1960–1974. The mixed layer
222 salinity then increases by ~ 0.6 psu between 1974 and 1993, followed by a sharp
223 decrease of ~ 0.7 psu between 1993 and 2012. It increases again after 2012. The
224 corresponding linear trends are -0.020 , 0.019 , and -0.024 psu/yr, about one order of
225 magnitude higher than the 56-year long-term trend (-0.004 psu/yr). All trends
226 reported here are statistically significant according to the t -test. The salinity change
227 rates in the mixed layer are about two to three times higher than those reported for the
228 subsurface layer by Zeng et al (2016a).

229 To explore the regional differences in mixed layer salinity variability, yearly
230 variations in the mixed layer salinity anomaly averaged over six well-sampled regions
231 are shown in Figure 9. The decadal timescale variability is similar for each region
232 with a salinification period that is slightly more noticeable in the northern basin than
233 in the southern basin.

234 **3.4 Mixed layer salinity variability and the PDO**

235 As the largest marginal sea in the northwest Pacific Ocean, the climate and
236 environment of the SCS are strongly influenced by the PDO. For example, a coral
237 geochemistry record in the northern SCS was reported to be significantly correlated
238 with the PDO index over the last century (Deng et al., 2013). In Figure 10, we
239 superimpose the mixed layer salinity anomaly on the PDO index and find that there is

240 a reasonably good agreement between the two curves.

241 The correlation between yearly mean mixed layer salinities and the PDO index is
242 0.45 at the 95% confidence level. Their correlation is much higher after the 1990s
243 than prior. The freshening periods generally coincide with a declining stage of the
244 PDO index, while the salinification periods are associated with an ascending stage.
245 The largest change in PDO index and mixed layer salinity occurs after 2012 when
246 both the mixed layer salinity and the PDO index rise quickly.

247 **4. Factors controlling variations in the mixed layer salinity**

248 What are the reasons for the salinification and freshening in the SCS mixed layer
249 salinity? In general, factors that can cause the mixed layer salinity changes include a)
250 net air-sea freshwater flux, b) the Luzon Strait transport induced horizontal salt
251 advection, and c) vertical entrainment and small-scale mixing processes. In this
252 section, we focus on the change in the surface freshwater flux and the surface current
253 during salinification/freshening periods (4.1); we then provide a more quantitative
254 assessment for each factor that contributes to the observed salinity change (4.2 and
255 4.3).

256 **4.1 Dry/wet conditions during salinification/freshening periods**

257 Figure 11a displays the spatial distribution of the long-term mean net surface
258 freshwater flux (color shading) based on the GPCP and mixed layer circulation
259 (vectors) based on the OFES model simulation. We use the GPCPflux dataset and the
260 OFES surface velocities because all of the datasets introduced in section 2 are

261 relatively consistent with each other. Over the 56-year period (Figure 11a),
262 evaporation is lower than precipitation in the SCS, except to the southwest of Taiwan.
263 There is also a clear signature of the Kuroshio intrusion across the Luzon Strait in the
264 SCS circulation.

265 Figures 11b-c show the change in the surface freshwater flux and the mixed layer
266 current for a salinification period (1974-1993) and a freshening period (1993-2012).
267 During the 1974-1993 salinification period (Figure 11b), the increasing trend of
268 freshwater loss dominates almost everywhere, except for the central northern SCS
269 where the freshwater flux is negative. In the surface circulation, there is an anomalous
270 westward flow trend east of the Luzon Strait (red vectors, Figure 11b) that, according
271 to Yu and Qu (2013), is an indication of a northward shift of the North Equatorial
272 Current (NEC) bifurcation, suggesting a stronger Kuroshio intrusion or larger Luzon
273 Strait transport. During the 1993-2012 freshening period (Figure 11c), the net
274 freshwater flux and ocean current distribution are opposite to that of the 1974-1993
275 salinification period. There is a decreasing trend of net freshwater loss across almost
276 the entire basin and the eastward flow trend east of the Luzon Strait is unfavorable for
277 Kuroshio intrusion (black vectors, Figure 11c). In summary, the trends of enhanced
278 (decreased) freshwater loss and Luzon Strait transport provide salinification
279 (freshening) conditions during a salinification (freshening) period.

280 Previous studies have shown that the PDO has an important influence on Asian
281 monsoon and monsoon precipitation. The PDO can either strengthen or weaken the

282 Walker circulation over the Indo-Pacific Ocean depending on the phase of the PDO
283 (Krishnamurthy and Krishnamurthy, 2014). For the SCS, during positive PDO phases
284 the descending motion of the Walker circulation leads to drought conditions over the
285 basin, while during negative phases the ascending motion brings heavy rainfall to the
286 SCS. The net freshwater loss is generally above average during the ascent PDO stage
287 and below average during the declining PDO stage, with exceptions occurring during
288 the mid-1990s and 2000s (Figure 12). Du et al. (2015) also reported a reduction in
289 freshwater loss in the southeastern tropical Indian Ocean starting from the mid-1990s
290 due to intensified Walker circulation. Yu and Qu (2013) found a significant imprint of
291 the PDO on decadal SCSTF variability. They indicated that during positive PDO
292 phases, the NEC bifurcation shifts northward and is responsible for the southward
293 intrusion of the Aleutian low, leading to a weaker Kuroshio and stronger SCSTF in
294 the upper 750 m. As shown in Figure 12, we find that the Luzon Strait transport
295 integrated within the mixed layer is also closely related to the PDO index and, in the
296 previous section, we showed that the averaged SCS mixed layer salinity variations are
297 in sync with the PDO.

298 **4.2 Box-average mixed layer salinity budget**

299 In this section, we address whether the contribution of freshwater flux and Luzon
300 Strait salt transport changes can fully account for the observed mixed layer salinity
301 variations. In order to quantify the factors affecting the mixed layer salinity in the
302 SCS, we perform a mixed layer salinity budget:

$$\Delta S_m = \underbrace{\frac{S_o \cdot (E - P - R) \cdot A_{SCS}}{V_{SCS}}}_{\text{Surface forcing}} + \underbrace{\frac{T_{in} \cdot \Delta S_{in}}{V_{SCS}} - \frac{T_{out} \cdot \Delta S_{out}}{V_{SCS}}}_{\text{Horizontal advection}} - \underbrace{\frac{\Gamma(w_e) \cdot (S_m - S_b)}{H}}_{\text{Vertical entrainment}} + \varepsilon \quad (1)$$

304 From left to right, the terms correspond to mixed layer salinity variations; surface
305 forcing (loss from ocean defined as positive); horizontal advection term (defined as
306 positive into the SCS), which contain advectons into (second term on right side) and
307 out of (third term) the basin; vertical entrainment; and a residual term, which includes
308 diffusion and other small effects. Here, S_m is mixed layer salinity, S_o is the mean sea
309 surface salinity, and A_{SCS} , H , and V_{SCS} are the surface area, mixed layer depth, and
310 volume of the SCS (111°–121°E, 16°–22°N), respectively. E is the evaporation, P is
311 the precipitation, and R is the river discharge; their net value is the net freshwater flux
312 out of the basin (loss from the ocean is defined as positive).

313 Accurately quantifying the horizontal advection over the entire basin is difficult.
314 For a basin-wide study, the horizontal salinity transport can be represented by two
315 components: inflow and outflow salt transport terms. Here, T_{in} and T_{out} are the volume
316 transports into and out of the basin, respectively, and ΔS_{in} (ΔS_{out}) is the salinity
317 difference between waters outside the inflow (outflow) straits and waters within the
318 SCS, where a positive transport term means an enhanced salinity effect. As mentioned
319 earlier, the exchange between the SCS and surrounding oceans consists mainly of
320 inflow from the Kuroshio through the Luzon Strait, and outflow primarily through the
321 Mindoro, Karimata, and Taiwan Straits (Yaremchuk et al., 2009). Because of the small
322 salinity contrast across the outflow straits, we disregard the outflow transport terms
323 when performing the budget.

324 The vertical processes contain vertical Ekman velocity and diapycnal mixing
 325 velocity (Michel et al., 2007). Following Michel et al. (2007) and Yu (2015), we have

$$326 \quad w_e = w_{Ek} + w_m = \frac{\nabla \times \tau}{\rho f} + \left(\frac{\partial H}{\partial t} + \nabla \cdot HU \right) \quad (2)$$

327 where τ denotes wind stress, ρ the mixed layer density, f the Coriolis frequency,
 328 and U includes Ekman and geostrophic current. The Ekman velocity w_{ek}
 329 corresponds to the upwelling (downwelling) generated by the convergence
 330 (divergence) of the horizontal Ekman transport (Yu, 2011). The mixing velocity w_m ,
 331 or the mixed layer depth tendency, can be influenced by wind, buoyancy, and other
 332 thermodynamic processes. In Eq. (1), Γ is the Heaviside function and w_e is the
 333 entrainment velocity at the bottom of the mixed layer; S_b is defined as the salinity at
 334 20 m below the mixed layer depth (Ren et al., 2011); Γ is used to represent
 335 entrainment ($w_e > 0$) and detrainment ($w_e < 0$) to the mixed layer. Only the
 336 entrainment of subsurface water affects the mixed layer salinity; detrainment removes
 337 mixed layer water but does not modify its salinity (Niiler and Kraus, 1977; Michel et
 338 al., 2007; Yu, 2015).

339 Thus, we have a simplified expression for the box-average mixed layer salinity
 340 variation:

$$341 \quad \Delta S_m = \frac{S_0 \cdot (E - P - R) \cdot A_{SCS}}{V_{SCS}} + \frac{LST \cdot \Delta S_{Lz}}{V_{SCS}} - \frac{\Gamma(w_e) \cdot (S_m - S_b)}{H} + \varepsilon \quad (3)$$

342 where ΔS_{Lz} is the salinity difference between two sides of the Luzon Strait, the
 343 Western Pacific water east of the Luzon Strait (S_{WP}) and the SCS (S_{SCS}).

344 **4.3 Factors controlling the mixed layer salinity variability**

345 To quantify the impact of the uncertainties associated with different data
346 products, we use several datasets (introduced in Section 2) for the freshwater flux and
347 the Luzon Strait transport to calculate the contribution of the surface forcing and
348 advection terms to the salinity budget. The time evolution of the budget terms are
349 displayed in psu/yr in Figure 13. The surface forcing and the horizontal advection
350 terms dominate and the vertical mixing is smaller by one order of magnitude. The
351 trends for each term during the freshening and salinification periods, using the
352 different datasets, are listed in Table 1.

353 During the 1960–1974 freshening period, the trends in the surface forcing,
354 advection, and entrainment terms were -0.011 , -0.006 and -0.0003 psu/yr,
355 respectively. Their total contribution was about -0.017 psu/yr, roughly equivalent to
356 the change in mixed layer salinity of -0.015 psu/yr. This result indicates that the
357 surface forcing and advection terms basically determine the freshening trend. It also
358 suggests that the effect of horizontal advection through the Luzon Strait is of similar
359 magnitude to that of the surface forcing term. During the 1974–1993 salinification
360 period, the surface forcing, advection, and entrainment terms all exhibit positive
361 trends, with values of 0.016 , 0.004 , and 0.0013 psu/yr, respectively. The sum of the
362 three terms, 0.021 psu/yr, is very close to the observed salinification trend of 0.023
363 psu/yr. This salinification is driven by enhanced surface freshwater loss and salt
364 transport through the Luzon Strait. In contrast to the 1960-1974 freshening period, the
365 surface forcing term is the dominant factor contributing to this salinification trend.

366 After the year of maximum salinity (1993), the surface forcing, advection, and
367 entrainment terms decrease again with negative trends of -0.010 , -0.010 , and -0.0008
368 psu/yr, respectively. The total impact of -0.021 psu/yr is close to the observed
369 freshening trend of -0.025 psu/yr. Similar as the 1960–1974 freshening period, the
370 surface forcing and advection terms basically determine the 1993–2012 freshening
371 period. Overall, though admittedly crude, this calculation is able to quantitatively
372 account for most of the observed mixed layer salinity changes (Figure 13d). In
373 summary, the mixed layer freshening is controlled by equal contributions from the
374 surface forcing and advection terms, while the surface forcing is the dominant term
375 for mixed layer salinification.

376 **5 Conclusion and Discussions**

377 In this paper, we examine the long-term variability of the mixed layer salinity in
378 the SCS over the past 56 years (1960–2015) using an in situ dataset (SCSPOD15) to
379 document the variability and a box-average salinity budget to quantify the factors
380 controlling these variations.

381 The mixed layer salinity exhibits significant variability on decadal and longer
382 timescales. During the 1960–2015 period, the mixed layer salinity freshens by more
383 than 0.2 psu, with an averaged trend of -0.20 psu/50yr (or -0.004 psu/yr). This
384 freshening trend is stronger in the northern basin than in the southern basin. The in
385 situ observations in the SCS show that it becomes fresher in the 1960s, starts to
386 salinify in 1974, freshens again from 1993, and then salinifies yet again in 2012, with

387 linear trends of -0.019 , 0.020 , and -0.024 psu/yr, respectively. These decadal salinity
388 change rates in the mixed layer are about two to three times larger than those in the
389 subsurface layer as reported by Zeng et al. (2016). We find that the long-term
390 variability in mixed layer salinity is in sync with the PDO. During the ascent
391 (declining) stage of the PDO, the ascending (descending) motion of the Walker
392 circulation leads to flood (drought) conditions over the basin, along with less (more)
393 intrusion of additional saline water by the Luzon Strait transport associated with a
394 stronger (weaker) Kuroshio; this results in freshening (salinification) in the SCS (see
395 schematic Figure 14).

396 Although the SCSPD15 dataset provides unprecedented observational coverage
397 in the SCS, there are still gaps and insufficient and uneven observations in some years.
398 One of the largest uncertainties in the trends assessment comes from the assembled
399 observational dataset. However, because we find that the observed mixed layer
400 salinity variability is in good agreement with the variability derived from a
401 box-average mixed layer salinity budget, we are confident that the trends reported
402 here are representative. The mixed layer salinity budget analysis is then used to
403 quantify the forcing factors controlling long-term changes in mixed layer salinity. The
404 results show that the freshening period is associated with a reduction in both the
405 surface freshwater loss and the Luzon Strait transport advection terms, while the
406 salinification period is mostly controlled by enhanced surface freshwater loss. While
407 we have assessed the uncertainty by utilizing as many surface forcing products and

408 ocean current outputs as possible (both with and without data assimilation), it is clear
409 that the accuracy of different surface forcing products and the realism of the ocean
410 model current outputs remains an issue.

411 Finally, the question of whether freshening or salinification can induce
412 significant climate change in the SCS depends on the magnitude of the trends. In
413 order to affect the climate and the thermohaline circulation, the salinity changes must
414 be sufficiently large, exceeding a threshold (Manabe and Stouffer, 1995; Wu et al.,
415 2004). Barreiro et al. (2008) showed that a freshwater input exceeding 0.3 Sv per
416 decade (a model-dependent value) can weaken the thermohaline circulation in the
417 North Atlantic. We are then led to ask what is the threshold that must be exceeded in
418 the SCS to significantly influence its thermohaline circulation? In the SCS, changes in
419 the mixed layer salinity regulates the mixed layer (Figure 15). The observed mixed
420 layer salinity freshening or salinification trends could constructively contribute to a
421 reduction or enhancement of the mixed layer density (Figure 15a). The shoaling or
422 deepening of the mixed layer depth generally coincides with a freshening or
423 salinification of the mixed layer salinity (Figure 15b). Variations in salinity
424 stratification that form a barrier layer have an important influence on climate (Maes et
425 al., 2002, 2005). For the SCS, there is no significant change in the barrier layer during
426 the salinification, but a shoaling mixed layer depth is associated with a slight increase
427 in the barrier layer during the two freshening periods (Figure 15c). A combination of
428 the relatively shallow mixed layer and stronger barrier layer during the freshening

429 period could lead to a strengthening of the ocean–atmosphere coupling in the SCS. A
430 realistic climate model and well-designed experiments are needed to answer these
431 questions. Future studies could examine long-term changes in salinity, the threshold
432 for major change, and detailed processes affecting the thermohaline circulation and
433 climate change.

434 **Acknowledgements:**

435 We benefited from several observational datasets and numerical results made freely
436 available, including the SCSPD dataset
437 (<https://figshare.com/s/e5327a334130cd44dc6a>), the OAFlux evaporation
438 (ftp://ftp.whoi.edu/pub/science/oaflux/data_v3), the PREC precipitation
439 (<http://www.esrl.noaa.gov/psd/data/gridded/data.prec.html>), the CPC precipitation
440 (<http://apdrc.soest.hawaii.edu/data/data.php>), the GPCP precipitation
441 (<http://www.esrl.noaa.gov/psd/data/gridded/data.gpcp.html>), the TRMM 3B43
442 precipitation (<http://mirador.gsfc.nasa.gov/cgi-bin/mirador/>), OFES outputs
443 (<http://apdrc.soest.hawaii.edu/data/data.php>), the SODA
444 (<http://sodaserver.tamu.edu/assim/>), the GODAS
445 (<http://www.esrl.noaa.gov/psd/data/gridded/data.godas.html>), and the HYCOM
446 (<http://hycom.org/dataserver/glb-reanalysis>). LZ is supported by the National Natural
447 Science Foundation of China (Nos. 41776025, 41476014, 41606030). EPC and XX
448 are supported by the NOAA Climate Program Office MAPP Program (award
449 NA15OAR4310088) and the NSF Physical Oceanography Program (award 1537136).

450

451

452 **References:**

- 453 Adler, R. F., G. J. Huffman, A. Chang, R. Ferraro, P. Xie, J. Janowiak, B. Rudolf, U.
454 Schneider, S. Curtis, D. Bolvin, A. Gruber, J. Susskind, P. Arkin, and E. Nelkin
455 (2003), The version-2 global precipitation climatology project (GPCP) monthly
456 precipitation analysis (1979-present), *J. Hydrometeor.*, 4, 1147-1167.
- 457 Anilkumar, N., Chacko, R., Sabu, P., & George, J. V. (2015). Freshening of Antarctic
458 bottom water in the Indian Ocean sector of southern ocean. *Deep Sea Research*
459 *Part II Topical Studies in Oceanography*, 118, 162-169.
- 460 Barreiro, M., Fedorov, A., Pacanowski, R., & Philander, S. G. (2008). Abrupt climate
461 changes: how freshening of the northern Atlantic affects the thermohaline and
462 wind-driven oceanic circulations. *Annual Review of Earth & Planetary Sciences*,
463 36(36), 33-58.
- 464 Boyer, T. P., S. Levitus, J. I. Antonov, R. A. Locarnini, and H. E. Garcia (2005),
465 Linear trends in salinity for the World Ocean, 1955–1998, *Geophys. Res. Lett.*, 32,
466 L01604, doi:10.1029/2004GL021791.
- 467 Carton, J. A., and B. S. Giese (2008), A reanalysis of ocean climate using simple
468 ocean data assimilation (SODA), *Mon. Weather Rev.*, 136, 2999–3017.
- 469 Chassignet, E. P., Hurlburt, H. E., Smedstad, O. M., Halliwell, G. R., Hogan, P. J., &
470 Wallcraft, A. J., et al. (2009). Global ocean prediction with the Hybrid Coordinate
471 Ocean Model (HYCOM). *Oceanography*, 22(2), 64-75.
- 472 Chen, M. Y., P. P. Xie, J. E. Janowiak, and P. A. Arkin (2002), Global land
473 precipitation: A 50-yr monthly analysis based on gauge observations, *J.*

474 Hydrometeorol., 3, 249–266.

475 Curry, R., Dickson, B., & Yashayaev, I. (2003). A change in the freshwater balance of
476 the Atlantic ocean over the past four decades. *Nature*, 426(6968), 826-829.

477 Delcroix, T., S. Cravatte, and M. J. McPhaden (2007), Decadal variations and trends
478 in tropical Pacific sea surface salinity since 1970, *J. Geophys. Res.*, 112
479 (C3) :266-281

480 Deng, W., G. Wei, L. Xie, T. Ke, Z. Wang, T. Zeng, and Y. Liu (2013), Variations in
481 the Pacific Decadal Oscillation since 1853 in a coral record from the northern
482 South China Sea, *J. Geophys. Res. Oceans*, 118, 2358–2366,
483 doi:10.1002/jgrc.20180.

484 Dickson, B., Yashayaev, I., Meincke, J., Turrell, B., Dye, S., & Holfort, J. (2002).
485 Rapid freshening of the deep north Atlantic ocean over the past four decades.
486 *Nature*, 416(6883), 832-7.

487 Du, Y., Y. Zhang., Ming Feng., T. Wang., N. Zhang, and S. Wijffels (2015), Decadal
488 trends of the upper ocean salinity in the tropical Indo-Pacific since mid-1990s. *Sci.*
489 *Rep.* 5, 16050; doi: 10.1038/srep16050 (2015).

490 Durack P. J., and S. E. Wijffels, (2010), Fifty-year trends in global ocean salinities and
491 their relationship to broadscale warming *J. Clim.* 23, 4342–4362

492 Durack, P. J., S. E. Wijffels, and R. J. Matear (2012), Ocean salinities reveal strong
493 global water cycle intensification during 1950 to 2000, *Science*, 336(6080), 455–
494 458, doi:10.1126/science.1212222.

495 Gordon, A. L., B. A. Huber, E. J. Metzger, R. D. Susanto, H. E. Hurlburt, and T. R.

496 Adi (2012), South China Sea throughflow impact on the Indonesian throughflow,
497 *Geophys. Res. Lett.*, 39 (11):117-128

498 Häkkinen, S., (2002), Freshening of the Labrador Sea surface waters in the 1990s:
499 Another great salinity anomaly? *Geophys. Res. Lett.*, 29(24) 2232, doi:
500 10.1029/2002GL015243

501 Holliday, N. P., Hughes, S. L., Bacon, S., Beszczynska-Möller, A., Hansen, B., &
502 Lavin, A., et al. (2008), Reversal of the 1960s to 1990s freshening trend in the
503 northeast North Atlantic and Nordic Seas, *Geophys. Res. Lett.*, 35(3), 3614

504 Huang, B. Y., Xue, Y., Zhang, D. X., Kumar, A., & Mcphaden, M. J. (2010). The
505 NCEP GODAS ocean analysis of the tropical Pacific mixed layer heat budget on
506 seasonal to interannual time scales. *Journal of Climate*, 23(18), 4901-4925.

507 Huffman, G. J., R. F. Adler., D. T. Bolvin., G. Gu., E. J. Nelkin., K. P. Bowman., Y.
508 Hong., E. F. Stocker., and D. B. Wolff., (2007), The TRMM multi-satellite
509 precipitation analysis: quasi-global, multi-year, combined-sensor precipitation
510 estimates at fine scale. *J. Hydrometeorol.* 8 (1), 38-55.

511 Krishnamurthy, L., and Krishnamurthy, V. (2014). Influence of PDO on south Asian
512 summer monsoon and monsoon–ENSO relation. *Climate Dynamics*, 42(9-10),
513 1-14.

514 Lau, K. M. (2009). East Asian summer monsoon rainfall variability and climate
515 teleconnection. *Journal of the Meteorological Society of Japan*, 70(1B), p211-242.

516 Liu, C., Wang, D., Chen, J., Du, Y., & Xie, Q. (2012). Freshening of the intermediate
517 water of the South China Sea between the 1960s and the 1980s. *Chinese Journal of*

518 Oceanology and Limnology, 30(6), 1010-1015.

519 Liu, Q., Huang, R., & Wang, D. (2012). Implication of the South China Sea
520 throughflow for the interannual variability of the regional upper-ocean heat content.
521 Adv. Atmos. Sci., 29(1), 54-62.

522 Li, L. R. W. Schmitt, C. Ummenhofer, K. Karnauskis, 2016. North Atlantic Salinity as
523 a Predictor of Sahel Rainfall. Science Advances, 2, e1501588.

524 Li, L., R. W. Schmitt, C. Ummenhofer, K. Karnauskis, 2016. Implications of North
525 Atlantic Sea Surface Salinity for Summer Precipitation over the US Midwest:
526 Mechanisms and Predictive Value. J. Climate, 29, 3143-3159.

527 Lukas, R., & Lindstrom, E. (1991). The mixed layer of the western equatorial Pacific
528 Ocean. Journal of Geophysical Research Atmospheres, 96(S01), 3343-3358.

529 Maes, C., J. Picaut, and S. Belamari (2002), Salinity barrier layer and onset of El Nino
530 in a Pacific coupled model, Geophys. Res. Lett., 29 (24), 59-1–59-4

531 Maes, C., J. Picaut, and S. Belamari (2005), Importance of salinity barrier layer for
532 the buildup of El Nino, J. Clim., 18, 104–118

533 Manabe, S., and Stouffer, R. J. (1995). Simulation of abrupt climate change induced
534 by freshwater input to the north Atlantic Ocean. Nature, 378(6553), 165-167.

535 Menezes, V. V., Macdonald, A. M., Schatzman, C (2017) Accelerated freshening of
536 Antarctic Bottom Water over the last decade in the Southern Indian Ocean. Sci.
537 Adv. 3, e1601426.

538 Michel, S., B. Chapron., J. Tournadre, and N. Reul (2007), Sea surface salinity
539 variability from a simplified mixed layer model of the global ocean. Ocean Science

540 Discussions, 4(1), 41-106.

541 Munk, W. (2003). Ocean freshening, sea level rising. *Science*, 300(5628), 2041-2043.

542 Nan, F., H. Xue, F. Chai, D. Wang, F. Yu, M. Shi, P. Guo, and P. Xiu (2013),
543 Weakening of the Kuroshio intrusion into the South China Sea over the past two
544 decades, *J. Clim.*, 26, 8097–8110.

545 Nan, F., Yu, F., Xue, H., Zeng, L., Wang, D., & Yang, S., et al. (2016). Freshening of
546 the upper ocean in the South China Sea since the early 1990s. *Deep Sea Research*
547 *Part I Oceanographic Research Papers*, 118, 20-29.

548 Niiler, P. P. and E. B. Kraus, One-dimensional models of the upper ocean, in
549 *Modeling and Prediction of the Upper Layers of the Ocean*, edited by E. B. Kraus,
550 Pergamon, New York, 325 pp., 143–172, 1977.

551 Qu, T., Du, Y., & Sasaki, H. (2006). South China Sea throughflow: A heat and
552 freshwater conveyor. *Geophysical Research Letters*. 332 (23): 430-452

553 Ren, L., K. Speer, and E. P. Chassignet (2011), The mixed layer salinity budget and
554 sea ice in the Southern Ocean, *J. Geophys. Res.*, 116 (C8): 239-255.

555 Sarafanov, A., A. Falina, A. Sokov, and A. Demidov (2008), Intense warming and
556 salinification of intermediate waters of southern origin in the eastern subpolar
557 North Atlantic in the 1990s to mid-2000s, *J. Geophys. Res.*, 113 (C12): 451-459.

558 Sasaki, H, M. Nonaka, Y. Masumoto, Y. Sasai, H. Uehara, and H. Sakuma (2007), An
559 eddy-resolving hindcast simulation of the quasi-global ocean from 1950 to 2003 on
560 the Earth Simulator. *High Resolution Numerical Modeling of the Atmosphere and*
561 *Ocean*, W. Ohfuchi and K. Hamilton, Eds., Springer, 157–185.

562 Schmitt, R. W., 1995. The ocean component of the global water cycle. U.S. National
563 Report to International Union of Geodesy and Geophysics, 1991–1994,
564 Supplement to Reviews of Geophysics, pp. 1395–1409.

565 Schmitt, R. W., 2008. Salinity and the Global Water Cycle. *Oceanography*, 21 (1),
566 12-19.

567 Schmitt, R. W. and A. Blair, 2015. A River of Salt. *Oceanography*, 28 (1), 40-45

568 Skliris, N., Marsh, R., Josey, S. A., Good, S. A., Liu, C., & Allan, R. P. (2014).
569 Salinity changes in the world ocean since 1950 in relation to changing surface
570 freshwater fluxes. *Climate Dynamics*, 43(3-4), 709-736.

571 Wang, B., Zhang, Y., & Lu, M. M. (2004). Definition of South China Sea monsoon
572 onset and commencement of the east Asia summer monsoon. *Journal of Climate*,
573 17(4), 699-710.

574 Wang, D., Q. Liu, R. X. Huang, Y. Du, and T. Qu (2006), Interannual variability of the
575 South China Sea throughflow inferred from wind data and an ocean data
576 assimilation product. *Geophys. Res. Lett.*, 33 (14): 110-118.

577 Wijffels, S., Schmitt, R., Bryden, H. & Stigebrandt (1992), A. Transport of freshwater
578 by the oceans. *J. Phys. Oceanogr.* 22, 155–162.

579 Wong, A. P. S., Bindoff, N. L. & Church, J. L. (1999), Large-scale freshening of
580 intermediate waters in the Pacific and Indian Oceans. *Nature* 400, 440–443

581 Wu, P., R. Wood, and P. Stott (2004), Does the recent freshening trend in the North
582 Atlantic indicate a weakening thermohaline circulation? *Geophys. Res. Lett.*, 31
583 (2) :2301

584 Xiu, P., F. Chai, L. Shi, H. J. Xue., and Y. Chao (2010), A census of eddy activities in
585 the South China Sea during 1993–2007. *J. Geophys. Res.*, 115, C03012, doi:
586 10.1029/2009JC005657.

587 Yaremchuk, M., J. McCreary Jr., Z. Yu, and R. Furue, 2009: The South China Sea
588 throughflow retrieved from climatological data. *J. Phys. Oceanogr.*, 39, 753–767

589 Yu, L., and R. A. Weller (2007), Objectively Analyzed Air–Sea Heat Fluxes for the
590 Global Ice-free Oceans (1981–2005). *Bull. Ameri. Meteor. Soc.*, 88, 527–539.

591 Yu, L. (2015), Sea-surface salinity fronts and associated salinity-minimum zones in
592 the tropical ocean, *J. Geophys. Res. Oceans*, 120(6), 4205–4225.

593 Yu, K., and T. Qu (2013), Imprint of the Pacific Decadal Oscillation on the South
594 China Sea throughflow variability, *J. Clim.*, 26(24), 9797–9805.

595 Zeng, L., W. T. Liu, H. Xue, P. Xiu, and D. Wang (2014), Freshening in the South
596 China Sea during 2012 revealed by Aquarius and in situ data, *J. Geophys. Res.*
597 *Oceans*, 119(12), 8296–8314.

598 Zeng L., D. Wang., P. Xiu., Y. Shu., Q. Wang and J. Chen., 2016, Decadal variation
599 and trends in subsurface salinity from 1960 to 2012 in the northern South China
600 Sea. *Geophysical Research Letter*, 43, 12181–12189

601 Zeng, L., D. Wang., J. Chen., W. Wang., and R. Chen (2016b), SCSPOD14, a South
602 China Sea physical oceanographic dataset derived from in situ measurements
603 during 1919–2014. *Sci. Data*, 3:160029 doi: 10.1038/sdata.2016.29

604 Zeng, L., Chassignet, E. P., Schmitt, R. W., Xu, X., and Wang, D. (2018).
605 Salinification in the South China Sea since late 2012: A reversal of the freshening

606 since the 1990s. *Geophysical Research Letters*, 45.

607 doi.org/10.1002/2017GL076574

608 Zhao, D., W. Wang., H. Qin., Q. Mao., D. Wang., and R. Chen (2014), Decadal

609 changes of the intermediate water at 18°N in the South China Sea. *Acta*

610 *Oceanologica Sinica* (in Chinese), 36(9): 56-64

611

612

613

614 Table 1: Long-term trends of each term in equation (3) in the SCS during the periods

615 1960–1974, 1974–1993, and 1993–2012. Units: psu/yr.

616

Mixed layer salinity trend	Surface forcing	Horizontal advection	Vertical entrainment	Sum of 3 terms	Observed trend
1960-1974	CPC:-0.014 PREC:-0.008 Mean:-0.011	SODA: -0.007 OFES: -0.006 Mean: -0.006	-0.0003	-0.017	-0.020
1974-1993	CPC:0.016 PREC:0.016 Mean:0.016	SODA: 0.002 OFES: 0.004 Mean: 0.003	0.0013	0.020	0.019
1993-2012	CPC:-0.011 PREC:-0.010 GPCP:-0.009 TRMM:-0.013 Mean:-0.010	SODA: -0.005 OFES: -0.006 GODAS:-0.009 ROMS:-0.010 HYCOM:-0.017 Mean:-0.010	-0.0008	-0.021	-0.024

617

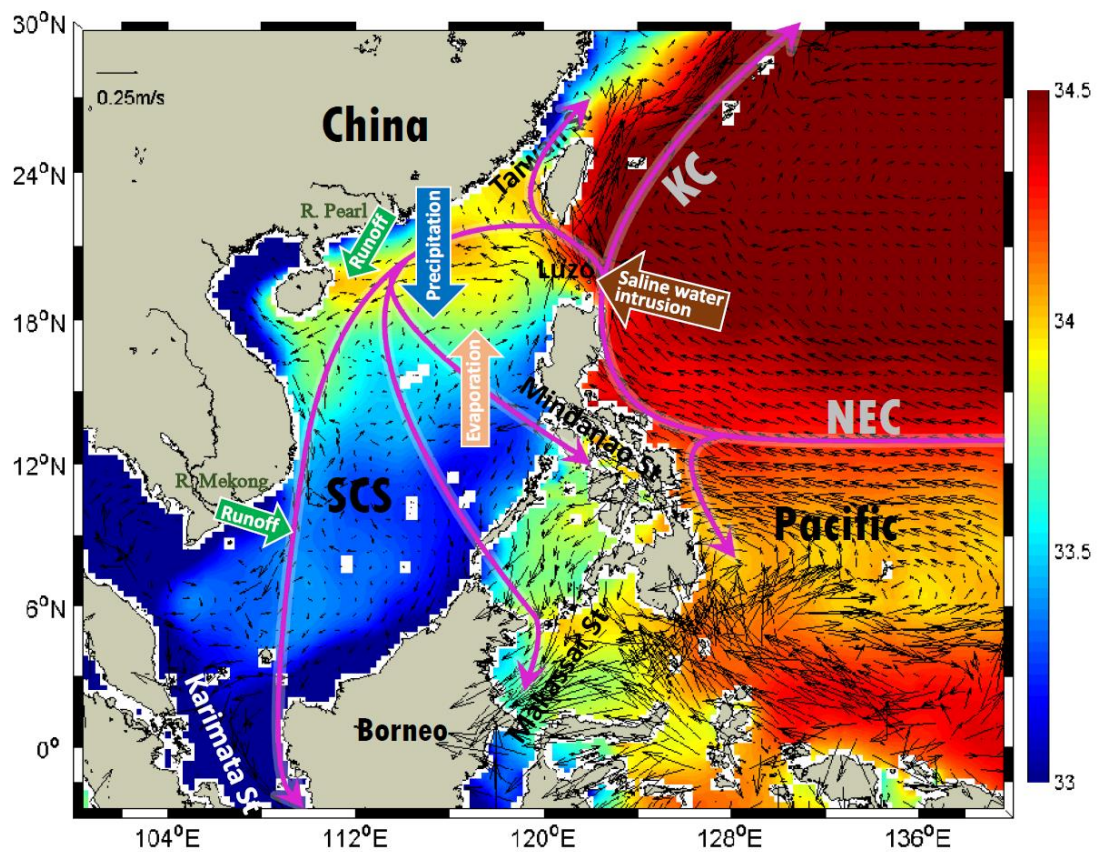
618

619

620

621

622

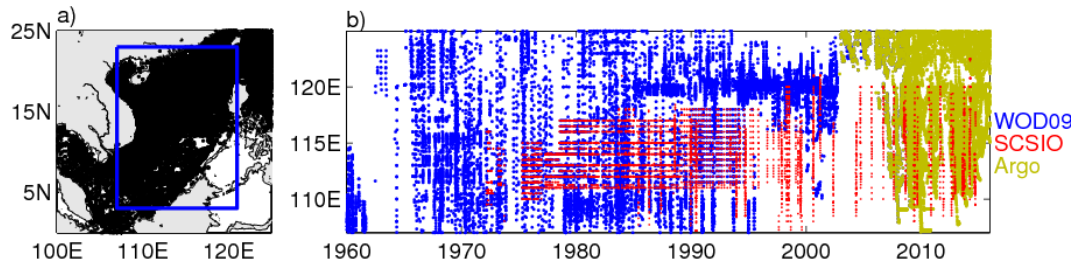


623

624

Figure 1. WOA13 mean surface salinity and OSCAR mean surface currents. Major
 625 currents in the SCS and adjacent waters are from Qu et al. (2006) and Hu et al. (2015),
 626 indicated by magenta lines. Abbreviations: SCS, South China Sea; NEC, North
 627 Equatorial Current; KC, Kuroshio Current.

628



629

630

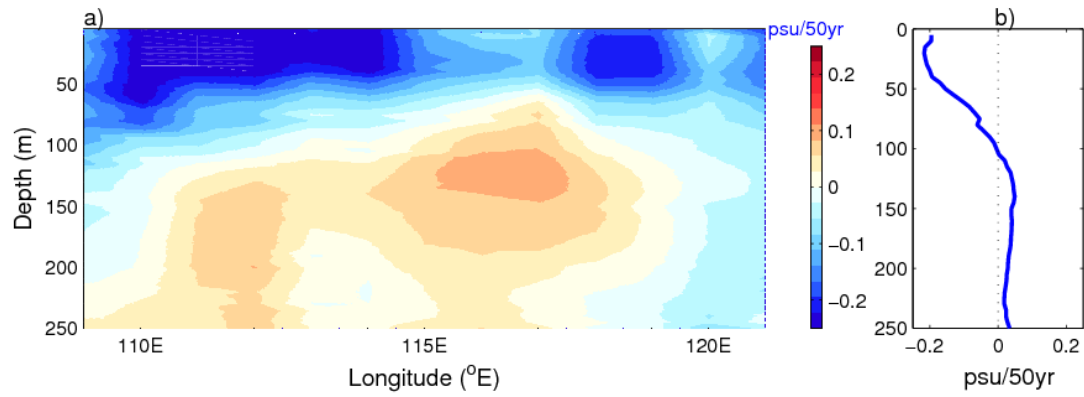
631

632

633

634

Figure 2. (a) Spatial distributions of observations from the SCSPOD15 dataset. The blue box represents the study area (SCS; 107–121°E, 3–23°N). (b) Longitude–time sections for the 3–23°N band of observations. The three data sources are marked by different colors: WOD09 (blue dots), SCSIO (red dots), and Argo (green dots).



635

636

Figure 3. Vertical distributions of upper salinity change (psu/yr) from 1960 to 2015 in

637

the SCS (basin area is defined as the region shown in Fig 2a). (a) Longitudinally

638

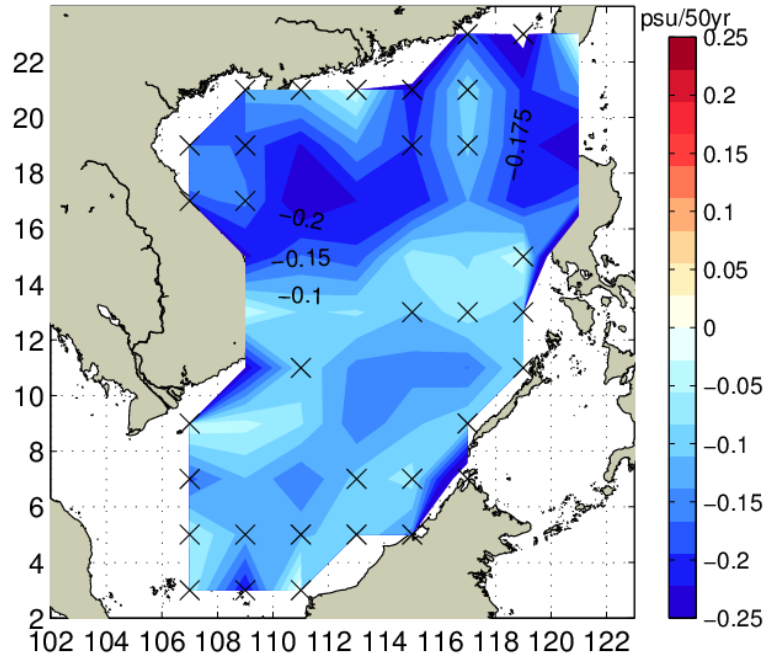
average and (b) basin-wide average for the SCS. In order to compare with the trend

639

identified by Durack et al. (2012), the unit is psu/50yr in this figure.

640

641



642

643 Figure 4. The linear trends in the mixed layer salinity calculated within each $2^{\circ} \times 2^{\circ}$

644 bins in the SCS. The cross delimits bins where the calculations of trends are not

645 reliable in Mann-Kendall test. In order to compare with the trend identified by Durack

646 et al. (2012), the unit is psu/50yr in this figure.

647

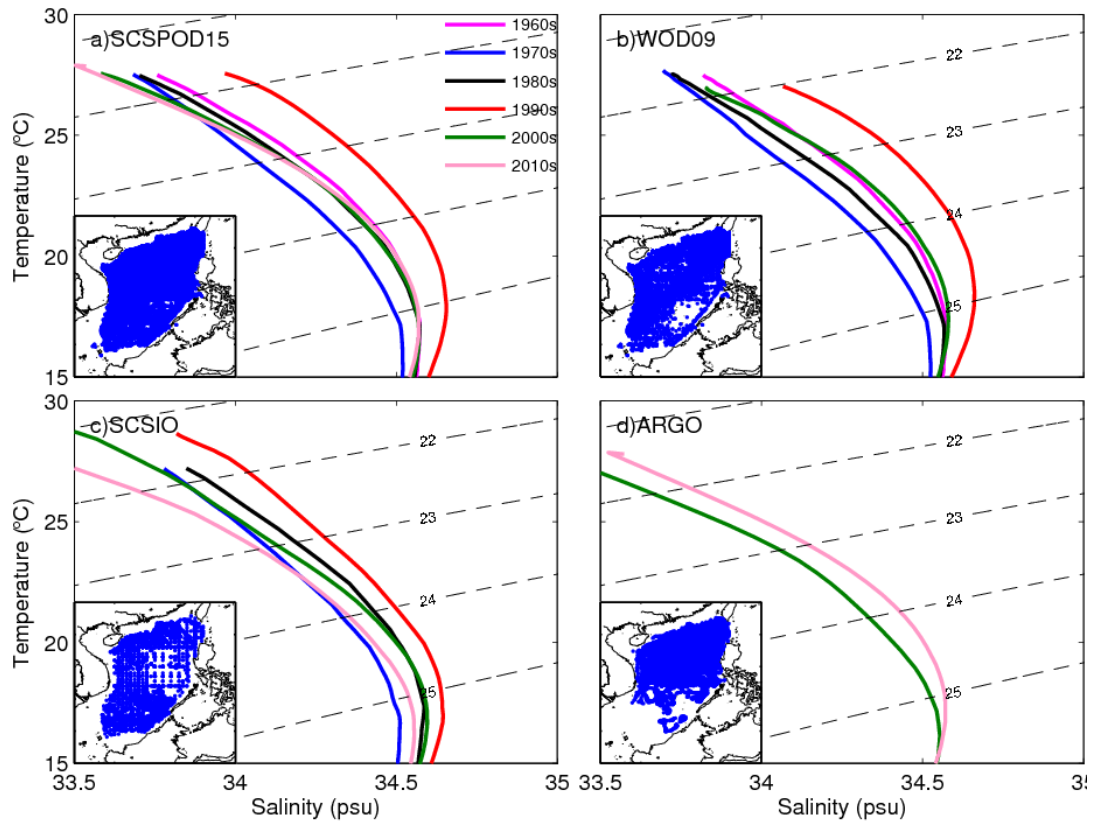
648

649

650

651

652



653

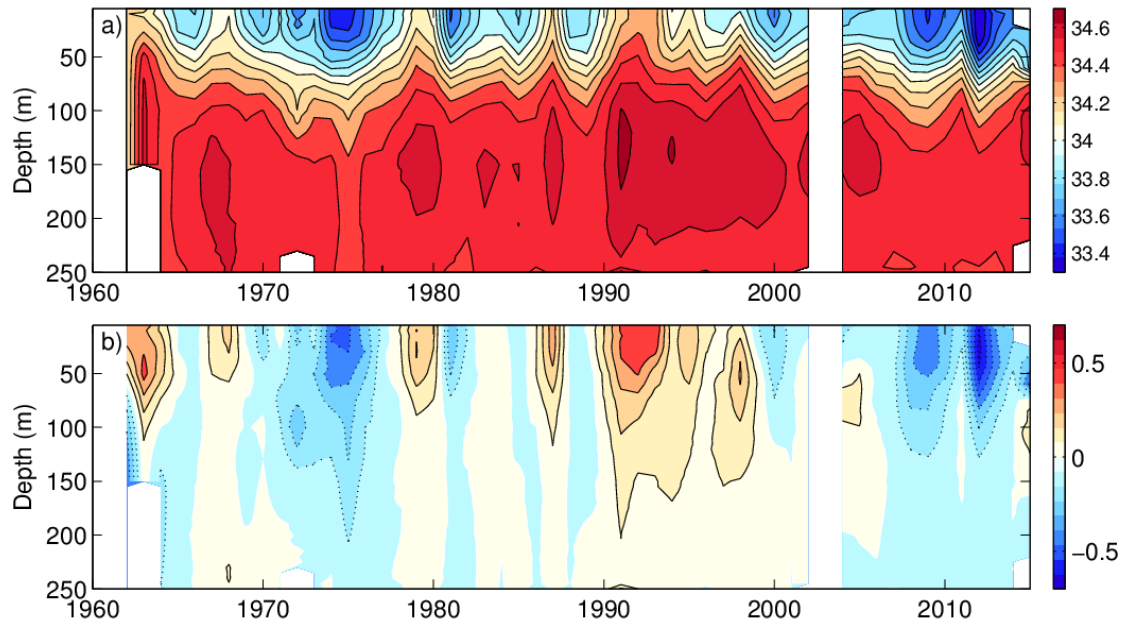
654

655

656

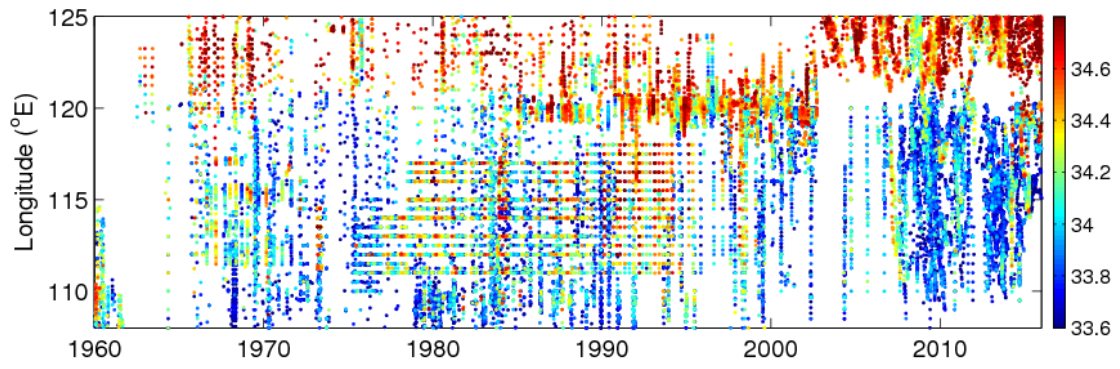
657

Figure 5. Decadal mean $T-S$ curves from 1960 to 2015 in the upper SCS (1960s: magenta; 1970s: blue; 1980s: black; 1990s: red; 2000s: green; 2010s: pink) based on, (a) SCSP0D15; (b) WOD09; (c) SCSIO; (d) Argo.



658

659 Figure 6. Time-depth sections of basin-wide averaged yearly mean (a) salinity, and (b)
 660 salinity anomalies (positive salinity anomaly: red; negative salinity anomaly: blue) in
 661 the upper SCS.
 662



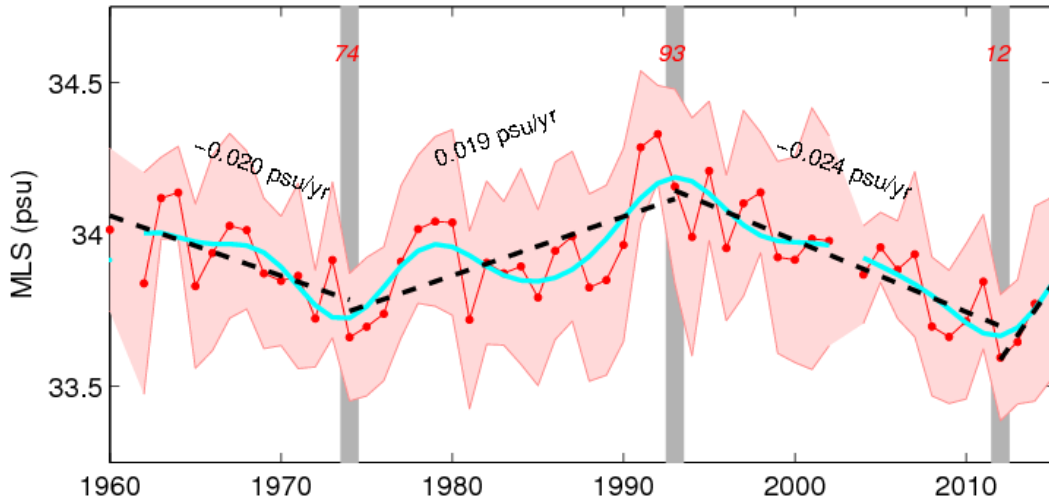
663

664

665

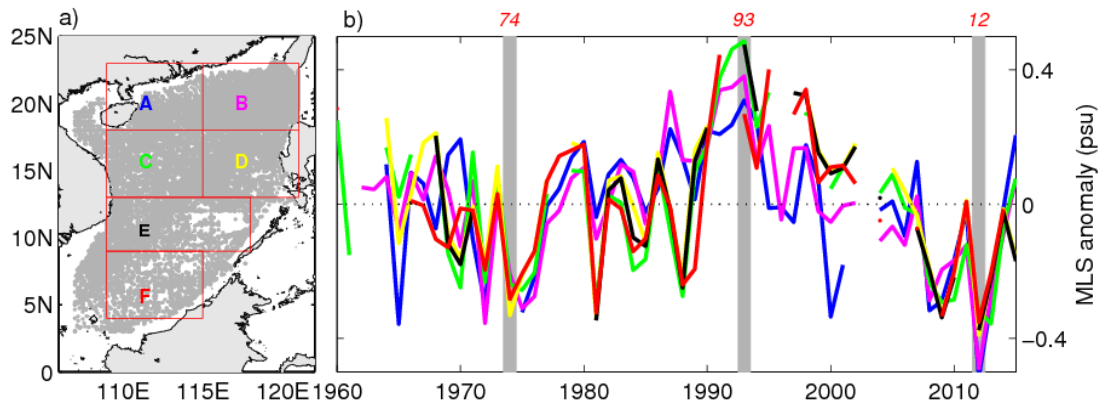
666

Figure 7. Longitude–time sections of mixed layer salinity (color, psu) for the 3–23°N band from 1960 to 2015 in the SCS.



667
 668
 669
 670
 671
 672
 673
 674
 675

Figure 8. Time series of average yearly basin-wide mixed layer salinity from 1960 to 2015 in the SCS. Shading (light red) indicates error bars. The error bar is estimated as the standard error of all mixed layer salinity values for a given calendar year. The low-frequency curve (blue) represents the seven-year filtered values used to highlight long-term changes. The dashed line represents the linear least squares fit of the yearly values used to quantify linear trends (psu/yr). The gray shaded areas indicate turning points in 1974, 1993, and 2012.



676

677 Figure 9. (a) Spatial distributions of selected SCSPOD15 observations in the study
 678 area (107–121°E, 3–23°N) and six selected areas (boxes) used for spatial averages. (b)
 679 Time series of yearly mixed layer salinity averaged in the six areas from 1960 to 2015
 680 in the SCS indicated by boxes in (a). The gray shaded areas indicate turning points in
 681 1974, 1993, and 2012.

682

683

684

685

686

687

688

689

690

691

692

693

694

695

696

697

698

699

700

701

702

703

704

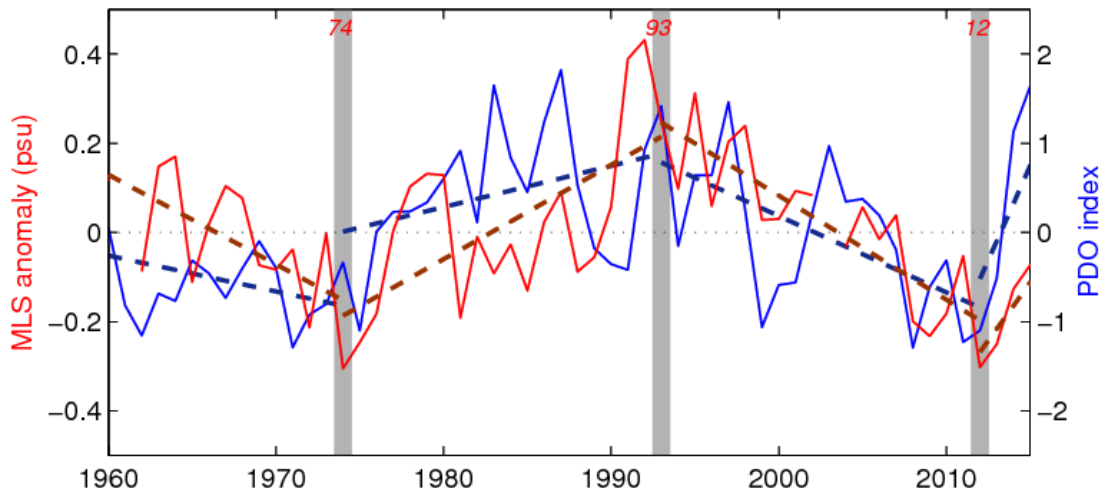
705

706

707

708

709



710

711 Figure 10. Time series of yearly PDO index (blue) and mixed layer salinity
 712 (red) in the SCS from 1960 to 2015. The gray shaded areas indicate turning points in
 713 1974, 1993, and 2012. The blue and red dashed line represents the linear least squares
 714 fit of the yearly values used to quantify linear trends for PDO and mixed layer salinity
 715 anomaly, respectively.

716

717

718

719

720

721

722

723

724

725

726

727

728

729

730

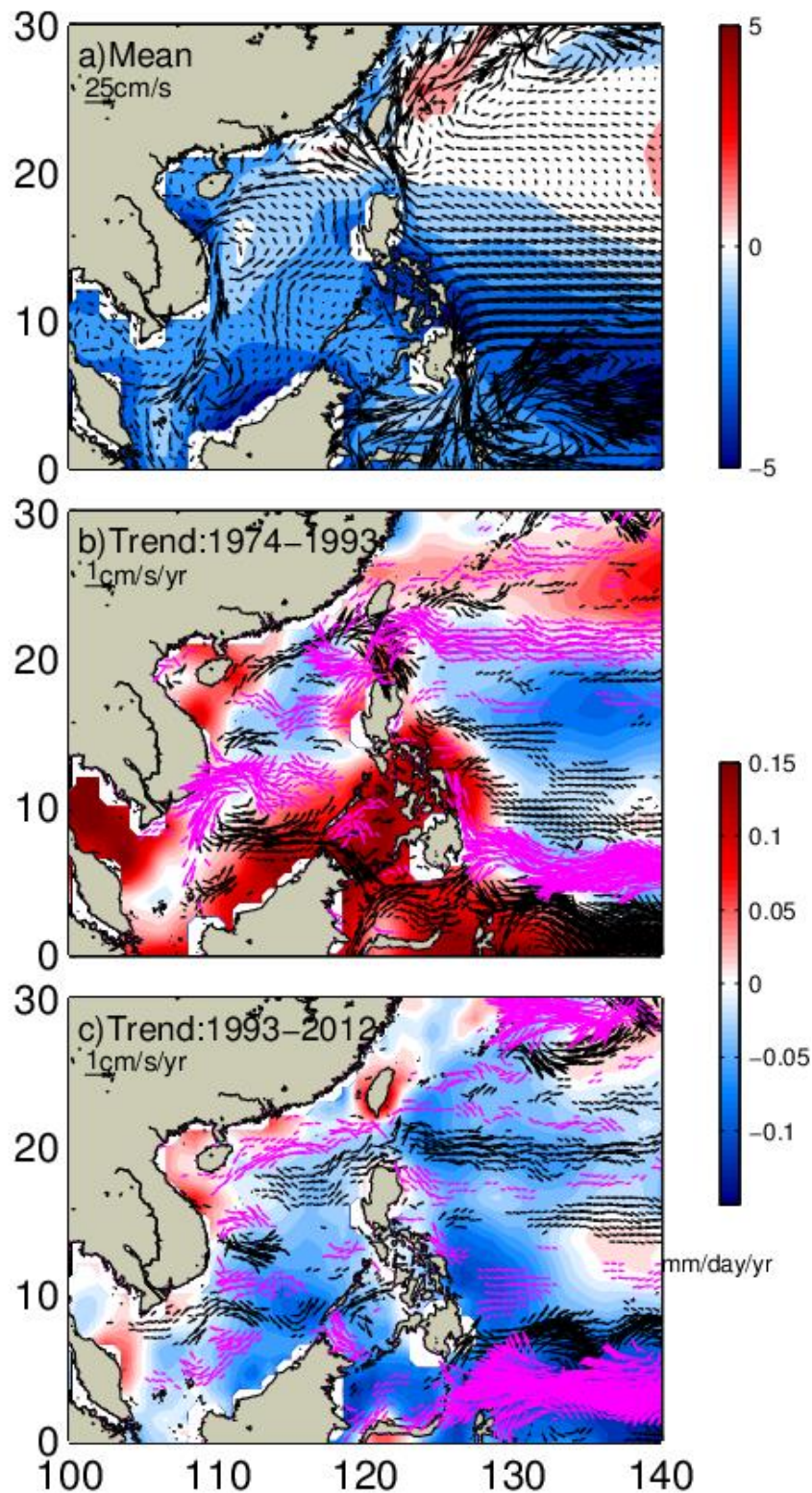
731

732

733

734

735



736

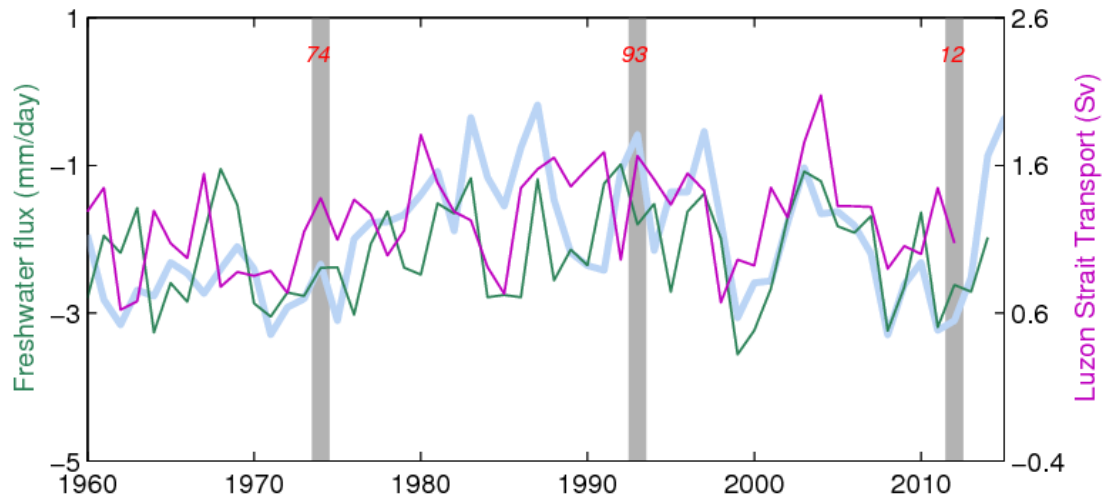
737 Figure 11. (a) Long-term mean GPCP freshwater flux ($E-P$, shading, unit: mm/d) and

738 OFES mixed layer circulation (vectors, unit: m/s). (b) Linear trend of GPCP

739 freshwater flux (shading, unit: mm/d/yr) and OFES circulation from 1974 to 1993

740 (magenta vectors: westerly currents; black vectors: easterly currents; unit: m/s/yr). (c)

741 Same as (b), but for the period 1993 to 2012.



742

743 Figure 12. Time series of yearly net freshwater flux ($E-P$, green, unit: mm/d), Luzon
 744 Strait transport (purple, unit: Sv) and yearly PDO index (light blue, PDO-2 is shown).

745 The gray shaded areas indicate turning points in 1974, 1993, and 2012.

746

747

748

749

750

751

752

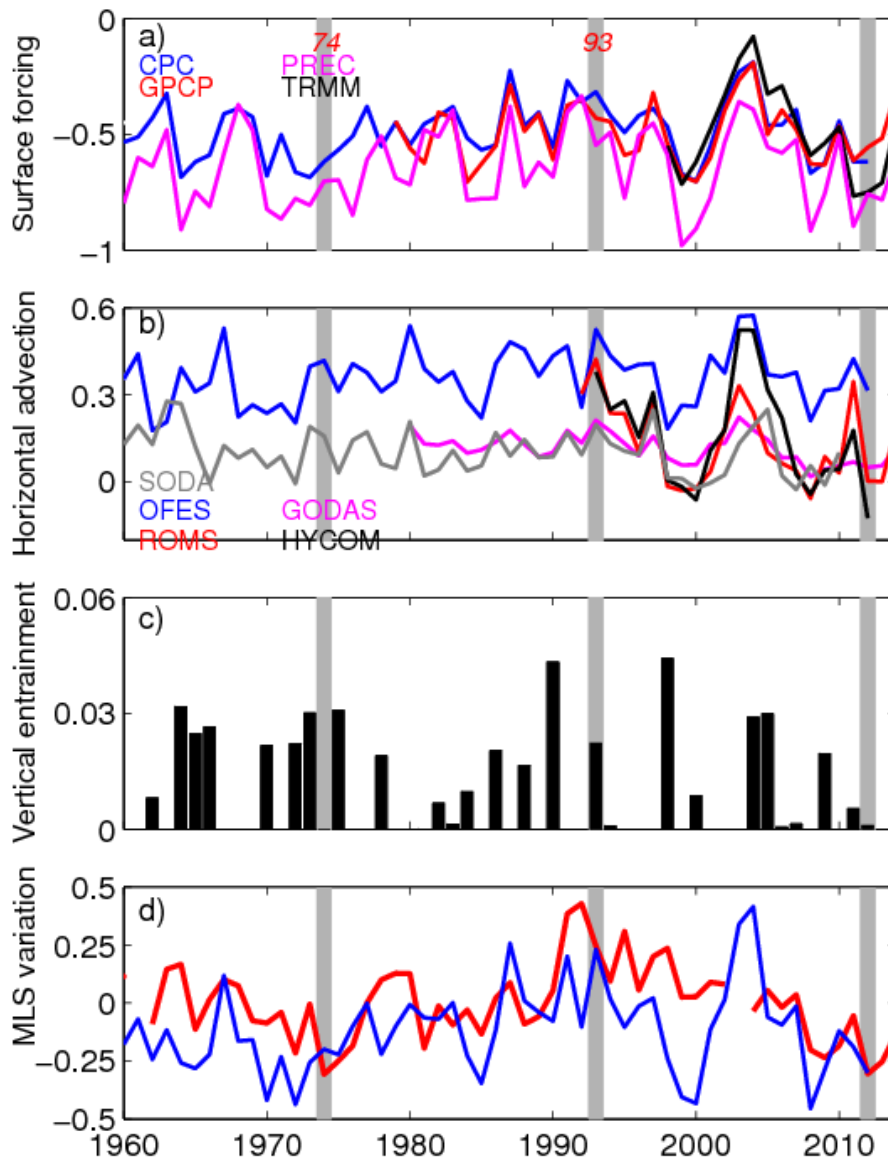
753

754

755

756

757



758

759 Figure 13. Spatial average of each term in equation (3) for the SCS (unit: psu/yr). (a)

760 Net freshwater flux term (CPCflux: blue; PRECflux: magenta; GPCPflux: red;

761 TRMMflux: black). (b) Luzon Strait transport induced horizontal advection term

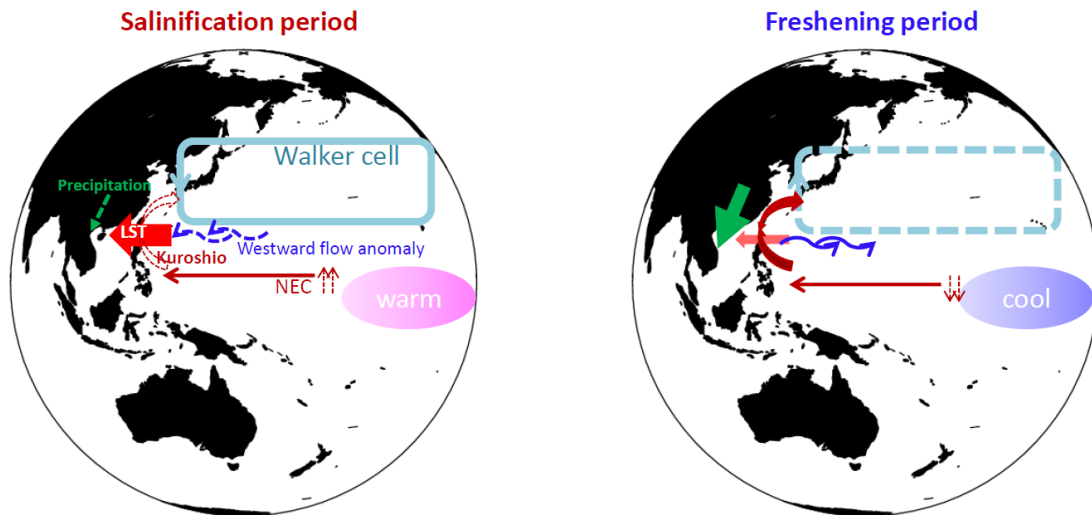
762 (SODAadv: gray; OFESadv: blue; GODASadv: magenta; ROMSadv: red;

763 HYCOMadv: black). (c) Vertical entrainment term. (d) Mixed layer salinity anomaly

764 variation, and the sum of the freshwater flux, horizontal advection, and vertical

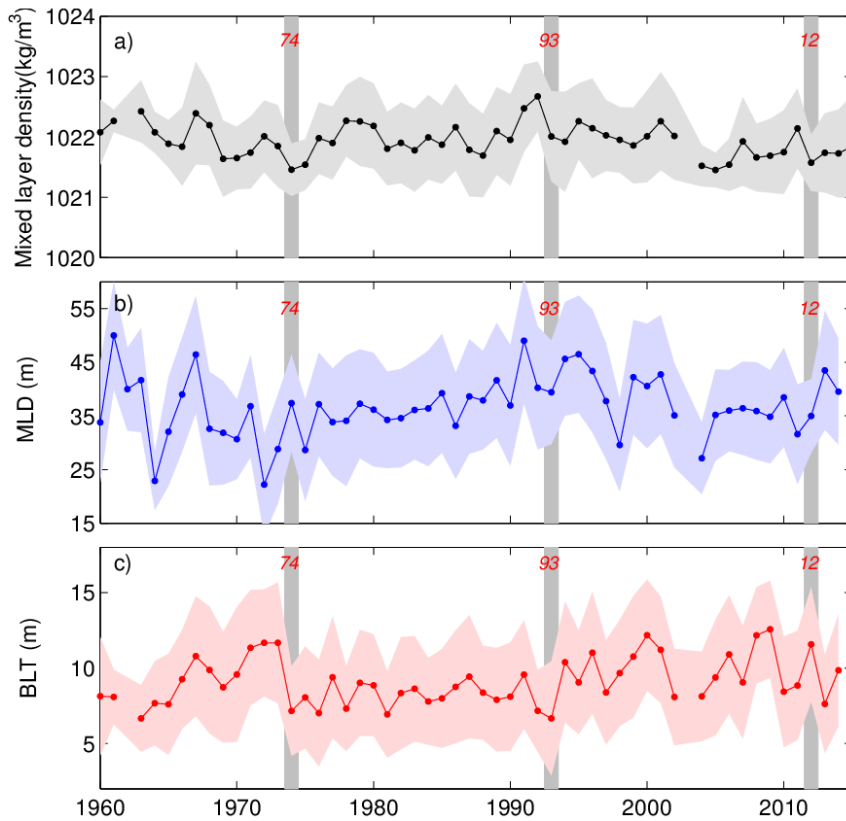
765 entrainment terms.

766



767
 768
 769
 770
 771
 772
 773
 774
 775
 776
 777
 778
 779
 780
 781
 782
 783
 784
 785
 786
 787
 788

Figure 14. Schematic diagram of the salinification (a) and freshening (b) periods in the SCS.



789 Figure 15. Time series of yearly (a) mixed layer density, (b) mixed layer depth, and (c)
 791 BLT averaged in the SCS. Error bars are shown in light shading. The gray shaded
 792 areas indicate turning points in 1974, 1993, and 2012.

789
 790
 791
 792
 793
 794
 795
 796
 797
 798
 799
 800
 801
 802
 803
 804
 805